



Experimental investigation on the energy and exergy performance of a coiled tube solar receiver

Jianqin Zhu^a, Kai Wang^{b,*}, Hongwei Wu^{c,*}, Dunjin Wang^b, Juan Du^b, A.G. Olabi^c

^a National Key Lab. of Science and Technology on Aero-Engines, School of Energy and Power Engineering, Beihang University, Beijing 100191, China

^b Institute of Engineering Thermophysics, Chinese Academy of Sciences, Beijing 100190, China

^c Institute of Engineering and Energy Technologies, School of Engineering and Computing, University of the West of Scotland, Paisley PA1 2BE, United Kingdom

HIGHLIGHTS

- Thermal performance of a coil type solar dish receiver is discussed.
- Energy and exergy analysis is performed for the overall system.
- The role of the heat loss factor is analyzed.
- The efficiency of energy and exergy are compared.
- The effect of temperature difference on exergy factor is explored.

ARTICLE INFO

Article history:

Received 10 February 2015

Received in revised form 29 May 2015

Accepted 4 July 2015

Keywords:

Solar receiver

Exergy

Energy efficiency

Heat transfer

Radiation

ABSTRACT

In this article, an experimental investigation is carried out to examine the heat transfer characteristics of a coil type solar dish receiver under actual concentrate solar radiation conditions. During the test, the concentrated solar flux is approximately 1000 kW/m^2 at aperture. The solar irradiance is almost unchanged (650 W/m^2) for continuous two hours in the afternoon, which is used to analyze the energy and exergy performance of the solar receiver. Experimental results show that, the efficiency of the solar receiver is normally above 70% with the highest efficiency of 82%, whereas at steady state, the efficiency is maintained at around 80%. A very low value of the heat loss factor (0.02 kW/K) could be achieved during the current steady state operating conditions. The highest value of the exergy rate is around 8.8 kW , whereas the maximum energy rate can reach 21.3 kW . In addition, the highest exergy efficiency is approximately 28%, and the highest energy efficiency is around 82%.

© 2015 Elsevier Ltd. All rights reserved.

1. Introduction

Nowadays, owing to the global progressively increasing demand for primary energy and the increasing scarcity of fossil energy sources, Concentrated Solar Power (CSP) system is considered as one of the most attractive ways to solve the energy crisis in the future [1]. A CSP plant uses the concentrated power of the sun as a heat source to generate mechanical power [2]. Many developed countries like the United State and the European Commission have done a lot of work on the solarised Brayton micro-turbines. The researches on the solar air receiver are done in three forms tower, trough and dish. In the framework of the

French PEGASE project (Production of Electricity by gas turbine and Solar Energy); CNRS/PROMES laboratory is developing a 4 MW pressurized air solar receiver with a surface absorber based on a compact heat exchanger technology [3]. ETH Zurich and Paul Scherrer Institute have done a field testing of a 42 m-long full-scale solar receiver prototype installed on a 9 m-aperture solar trough concentrator, the receiver efficiency ranges from 45% to 29% for a solar power input of 280 kW [4–6]. Comparing to the parabolic trough system with the concentration ratio of 100 suns and the central tower system with the concentration ratio of 1000 suns, the parabolic dish system can achieve concentration ratio of 10,000 suns. According to this, very high efficiency can be achieved in a parabolic dish solar system due to its high concentration ratio [7]. The solar concentration part which is used to provide high temperature air is very crucial for the entire solar power system. The system efficiency and the cost of power generation are highly

* Corresponding authors. Tel.: +86 (10)82543147; fax: +86 (10)82613328 (K. Wang). Tel.: +44 (0)1418483684; fax: +44 (0)1418483663 (H. Wu).

E-mail addresses: wang_kai@iet.cn (K. Wang), hongwei.wu@uws.ac.uk (H. Wu).

and different affect factors. It would be very helpful to improve the original design and predict the thermal performance of the optimized design.

It appears from the previous investigation that the key point for the solarised Brayton micro-turbines is to develop solar receivers which have terrific performance on the pressure loss and heat transfer. Most of the research works have been done by both the numerical and theoretical aspects. However, limited experimental study was done in the laboratory under constant solar radiation. There is a lack of available experimental data under real concentrate solar conditions especially for the cases of extremely high heat flux and high temperature. It is known that the real environmental condition is very complex since the solar radiation changes with time and the wind has great effect on the heat loss. This is strongly depended on the test season and location, in addition, the shadow of the cloud could cause heat shock in a short time. These impact factors could make the solar receiver working under unsteady condition. Therefore, to investigate the different impact factors on the achievement of better performance of the receiver becomes a very important issue. As such, the present work aims to analyze both the efficiency and heat loss of a coiled tube under real solar radiation conditions in a systematic manner. The obtained solar radiation data could be used as the boundary condition for future numerical simulation.

2. Experimental apparatus and method

2.1. Experimental apparatus

A new experimental test rig is constructed at a center with the geographical position of 38°23' latitude and 109°9' longitude. It is located about 15 km South of Yinchuan, the capital city of the autonomous region Ningxia of the People's Republic of China. A simplified schematic of the unit assembled for use in the

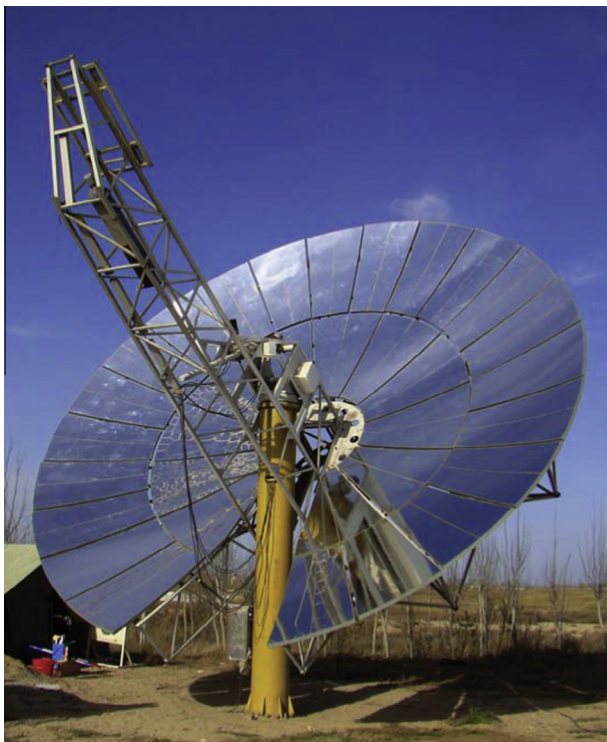


Fig. 1a. Parabolic dish.

experiments is depicted in Fig. 1a. The main components of the system consisted of dish, compressor and receiver.

The dish used for the experimental tests of the developed solar heat receiver is shown in Fig. 1b. All 33 trapezoidal, pre-bent mirrors are resin molded and laminated. The reflective surface is applied as an adhesive foil. At the bottom side of the dish a cut out is made for the tower. The main dish parameters utilized in the current study are illustrated in Table 1. To make sure the light reflected by the mirror focus on the aperture of the receiver, each mirror was adjusted individually. The dish is controlled by a solar tracker which is embedded in the inner program to make the dish face the Sun automatically. An uninterruptible power supply (UPS) system is also adopted to assist the dish off the solar direction in some emergency to further protect the receiver.

In the current test, a piston compressor is driven by a diesel engine with the power of 25 kW. The pressurized air is compressed at environmental temperature and pressure. After the filter, the pressurized air is supplied into the receiver. A valve is installed at the pipe outlet to ensure the receiver works under high pressure. By adjusting this valve, the pressure of the whole system as well as the portion of the receiver can be well controlled. The output mass flow rate (\dot{m}) is 0.045 kg/s. Thermocouple and pressure sensor are placed at the inlet and outlet of the pipe respectively to obtain the receiver efficiency and heat loss. The receiver itself is mounted onto the cantilever arm. To protect the receiver from misaligned radiation an additional steel plate is mounted circumferentially to the aperture.

2.2. Solar receiver model

For the current experimental evaluation, the solar is designed as a type of coiled tube, as shown in Fig. 2a. The section view of the solar receiver is shown in Fig. 2b. The pressured air is injected into the inlet tube with the diameter of 80 mm. And then, it is divided into 12 small tubes with the diameter of 14 mm. The 12 small tubes are welded into a cylinder which forms the main part of the solar receiver. The diameter and the height of the main part of the receiver are 250 mm and 456 mm, respectively. The overall dimensions of the receiver are confined by the size of the solar dish arm frame. Prior to the real test, preliminary and optimized analysis were conducted to select the diameter of the inlet tube (80 mm). The selected tube could ensure the pressure distribution in the 12 small tubes is equal, and the mass flow rate within each of the 12 small tubes is nearly same. The area of the inlet tube is more than 2.5 times of the total area of the 12 small tubes. The equal distribution of the mass flow is crucial in the design of the solar receiver. The optimized wall thickness of the tube has been done in our previous work [28]. The concentrate solar radiation (CSR) passes through the aperture and heat the inner surface of the core. To avoid the stress induced by thermal expansion, the 12 small tubes are arranged with a 5 mm clearance. All the small tubes combine together in the cone-type collector, and then connect with the outlet tube. A stainless steel is selected for making the receiver because of its strength at high temperature (900 °C). Between the tube and the case, it is stuffed with chamotte whose heat conductivity coefficient is 0.6 W/m² K⁻¹. The chamotte can be used to fix the tube and also acted as the thermal insulator to minimize the heat loss.

2.3. Energy and exergy analysis

Experimental energy and exergy parameters to characterize the thermal performance of the receiver are presented in this section [29]. Fig. 3a shows all the energy and exergy terms considered in

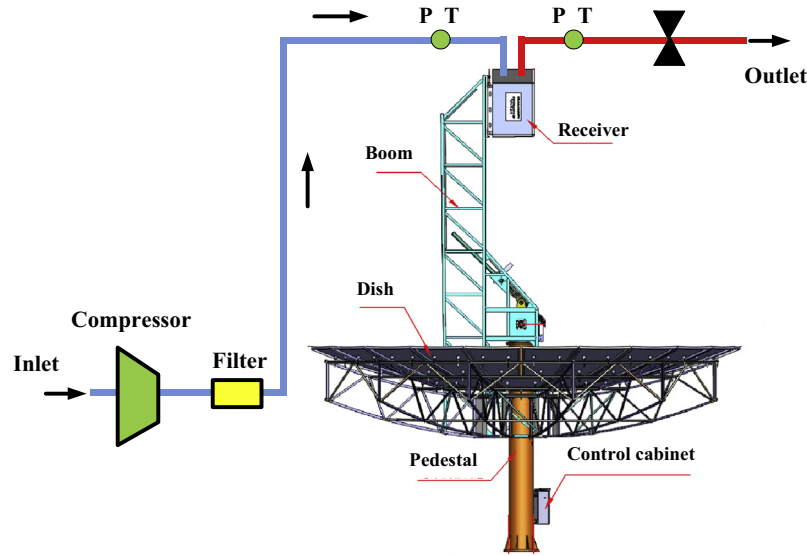


Fig. 1b. Schematic of the receiver test arrangement.

Table 1
Dish design parameters.

Parameters	Value (unit)
Effective aperture area of dish (A_{ap})	56.8 m ²
Project area (A_p)	54.4 m ²
Focus point diameter (D_f)	0.2 m
Concentration ratio (r_c)	1731
Parabolic dish combined optical efficiency (η_d)	73%

the overall system. Fig. 3b shows the Sankey diagram of the energy and exergy flows in the afternoon condition.

2.3.1. Energy analysis

The energy that the whole system receives comes from the solar radiation. The solar radiation power on the parabolic dish reflector can be expressed as:

$$E_S = A_{ap}G \quad (1)$$

where E_S is the solar radiation power on the dish, A_{ap} is the effective aperture area of the parabolic dish, as shown in Table 1. G is the direct solar irradiation from the Sun to the dish. G is measured with a normal incidence pyrheliometer (NIP) Hukseflux DR01 attached to the solar tracker. The G value can be recorded to monitor the variation of the solar irradiation in the whole day.

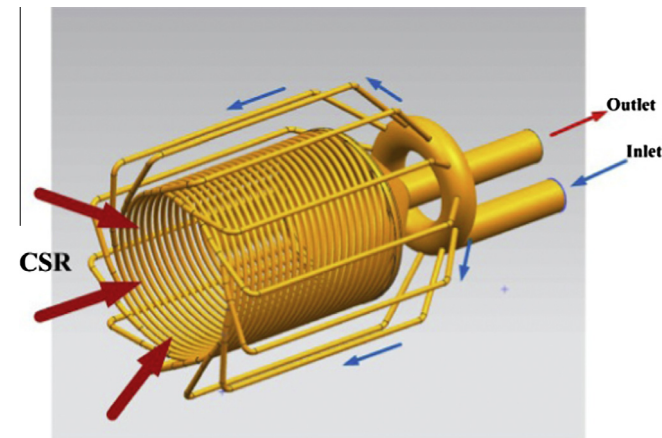


Fig. 2a. 3D model of the solar receiver.

The solar radiation is concentrated and delivered to the receiver by the parabolic dish. The concentrated solar radiation power (E_D) can be expressed as:

$$E_D = \eta_d E_S = \eta_d A_{ap}G \quad (2)$$

where E_D is the concentrated solar radiation power from parabolic dish to the receiver, η_d is the parabolic dish combined with optical efficiency with the value of 73% as described in Table 1. In the current study, η_d is given by the parabolic dish manufacturer and strongly depends on the situation of mirror.

The concentrated solar radiation on the receiver is absorbed by the heat-transfer fluid flowing in the tubes of the receiver. The energy rate that air absorbs or receives power is given by:

$$E_R = \dot{m}c_{av}(T_{out} - T_{in}) \quad (3)$$

where \dot{m} is the mass flow rate of the air, c_{av} is the average specific heat capacity of the air which is a function of the average air inlet temperature (T_{in}) and air outlet temperature (T_{out}). The average temperature of the receiver (T_{ave}) can be defined by:

$$T_{ave} = (T_{in} + T_{out})/2 \quad (4)$$

Thus, the relation between the average specific heat capacity of the air and the average temperature can be obtained as:

$$c_{av} = 0.9956 + 0.000093T_{ave} \quad (5)$$

Based on energy conservation, the receiver power is the difference between the concentrated solar radiation power and the overall heat losses that are not very high. The receiver power can also be described as:

$$E_R = E_D - E_L \quad (6)$$

where E_L is the rate of the heat loss from the receiver to the surroundings that can be expressed as:

$$E_L = U_L A_R (T_{ave} - T_{amb}) \quad (7)$$

where U_L is the heat loss coefficient determined, A_R is the effective receiver area, and T_{amb} is the ambient temperature recorded by a thermometer. During the experiment, the ambient temperature is maintained at around 10 °C. The product $U_L A_R$ is referred as the heat loss factor given by:

$$U'_L = U_L A_R \quad (8)$$

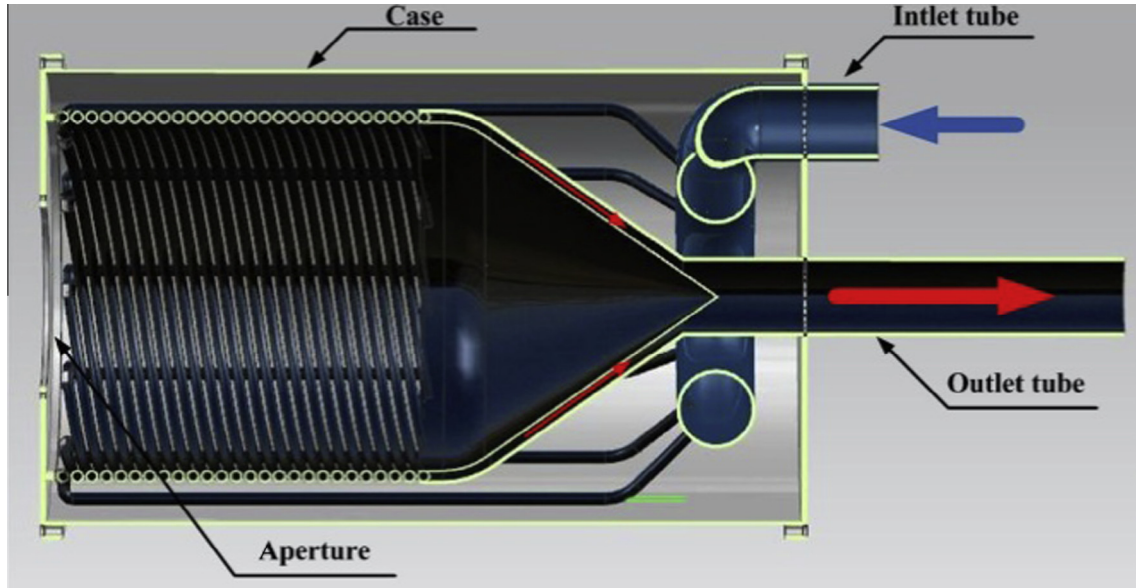


Fig. 2b. Section view of the solar receiver.

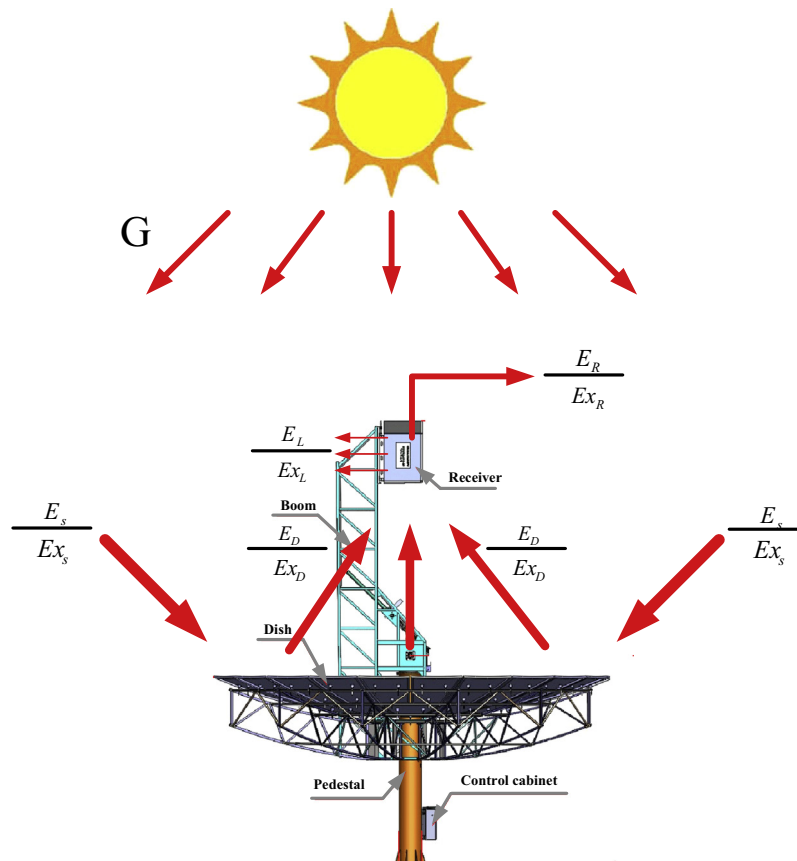


Fig. 3a. Schematic of the energy/exergy balance.

Therefore, combination of Eqs. 2, 3, 6 and 7 can yield

$$\dot{m}c_{av}(T_{out} - T_{in}) = n_d A_{ap} G - U'_L (T_{ave} - T_{amb}) \quad (9)$$

The thermal energy efficiency of the receiver is defined as the ratio of the receiver power to the concentrated solar radiation power from the parabolic dish to the receiver which is expressed as:

$$\eta_{th,R} = \frac{E_R}{E_D} = \frac{\dot{m}c_{av}(T_{out} - T_{in})}{n_d A_{ap} G} \quad (10)$$

It should be pointed out that the thermal energy efficiency is used to evaluate the heat absorbing ability of the solar receiver, thus, the total energy input to the solar receiver (E_D) is used to calculate $\eta_{th,R}$.

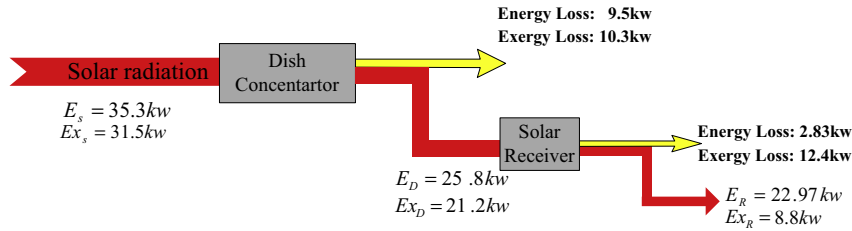


Fig. 3b. Sankey diagram of the energy and exergy flows in the afternoon condition.

By dividing A_{ap} on both side of Eq. (9) and combine with Eq. (10) leads to

$$\eta_{th,R} n_d = n_d - \frac{U'_L (T_{ave} - T_{amb})}{A_{ap} G} \quad (11)$$

2.3.2. Exergy analysis

The exergy rate of the receiver or the quality of the energy delivered to the circulating fluid with reference to the surroundings can be expressed as [30].

$$Ex_R = E_R - \dot{m} c_{av} T_{amb} \ln \left(\frac{T_{out}}{T_{in}} \right) \quad (12)$$

where Ex_R is the exergy rate of the receiver and $\dot{m} c_{av} T_{amb} \ln \left(\frac{T_{out}}{T_{in}} \right)$ is the exergy loss to the surroundings.

Substituting Eq. (3) into Eq. (12) yields

$$Ex_R = \dot{m} c_{av} \left[(T_{out} - T_{in}) - T_{amb} \ln \left(\frac{T_{out}}{T_{in}} \right) \right] \quad (13)$$

The rate of the solar exergy delivery by the Sun to the dish and then to the concentrator is given by the Petela [31] and is expressed as:

$$Ex_s = GA_{ap} \left[1 + \frac{1}{3} \left(\frac{T_{amb}}{T_s} \right)^4 - \frac{4T_{amb}}{3T_s} \right] \quad (14)$$

where T_s is the surface temperature of the Sun which is approximately 5762 K.

And the exergy rate translated from the dish concentrator to the receiver is expressed as:

$$Ex_D = n_d GA_{ap} \left[1 + \frac{1}{3} \left(\frac{T_{amb}}{T_s} \right)^4 - \frac{4T_{amb}}{3T_s} \right] \quad (15)$$

The exergy efficiency is used to evaluate the exergy converting ability of the solar receiver. The exergy efficiency is defined as the ratio of the receiver exergy rate (output exergy from the solar receiver) to the rate of the solar exergy (input exergy to the solar receiver) and can be determined as follows:

$$\eta_{ex,R} = \frac{Ex_R}{Ex_D} = \frac{\dot{m} c_{av} \left[(T_{out} - T_{in}) - T_{amb} \ln \left(\frac{T_{out}}{T_{in}} \right) \right]}{n_d GA_{ap} \left[1 + \frac{1}{3} \left(\frac{T_{amb}}{T_s} \right)^4 - \frac{4T_{amb}}{3T_s} \right]} \quad (16)$$

The exergy factor, which is defined as the ratio of the receiver exergy rate to the receiver energy rate, is expressed as follows:

$$Ex_f = \frac{Ex_R}{E_R} = \frac{\dot{m} c_{av} \left[(T_{out} - T_{in}) - T_{amb} \ln \left(\frac{T_{out}}{T_{in}} \right) \right]}{\dot{m} c_{av} (T_{out} - T_{in})} \quad (17)$$

3. Uncertainty analysis

The uncertainties of the measurement in the experiment are dependent on the experimental conditions and the measurement

instruments. An uncertainty analysis is performed on the receiver power E_R and the receiver exergy Ex_R , which are the most important derived quantities from the measurements of using the propagation of error method described by Moffat [32]. The uncertainty of the receiver power is calculated using the following equation:

$$\delta E_R = \sqrt{\left(\frac{\delta E_R}{\delta \dot{m}} \right)^2 (\delta \dot{m})^2 + \left(\frac{\delta E_R}{\delta T_{out}} \right)^2 (\delta T_{out})^2 + \left(\frac{\delta E_R}{\delta T_{in}} \right)^2 (\delta T_{in})^2} \quad (18)$$

While the uncertainty of the receiver exergy rate is given by:

$$\delta Ex_R = \sqrt{\left(\frac{\delta Ex_R}{\delta \dot{m}} \right)^2 (\delta \dot{m})^2 + \left(\frac{\delta Ex_R}{\delta T_{out}} \right)^2 (\delta T_{out})^2 + \left(\frac{\delta Ex_R}{\delta T_{in}} \right)^2 (\delta T_{in})^2 + \left(\frac{\delta Ex_R}{\delta T_{amb}} \right)^2 (\delta T_{amb})^2} \quad (19)$$

In the current study, the main uncertainty parameters are the mass flow rate (\dot{m}), the inlet temperature (T_{in}), and the outlet temperature (T_{out}). The relative uncertainty of the mass flow rate is 2%. Therefore, $\delta \dot{m} = 2\% \times \dot{m} = \pm 0.0009$ kg/s. The uncertainty of the temperature is given by the K-type thermocouple with the value of $\delta T_{out} = \delta T_{in} = \pm 0.5$ K.

Substituting, $\delta \dot{m}$, δT_{in} and δT_{out} into Eqs. (18) and (19). The maximum experimental values for the receiver power and exergy rate are around 21 kW and 8.5 kW, respectively. The uncertainty of the receiver power is 0.52 kW, and the uncertainty of the receiver exergy rate is 0.15 kW. Overall, the overall uncertainty of the receiver power and exergy rate are 2.5% and 1.8%, respectively.

4. Results and discussion

Fig. 4 shows the measured solar irradiance (G) plotted with respect to the testing time. The experimental data were collected on April 15th, 2014. For the purpose of comparison, in this study, experiments are done for two different time slots: morning (Fig. 4a) and afternoon (Fig. 4b). Fig. 4a shows the variation of the solar irradiance from 7:00 am to 11:30 am. According to the

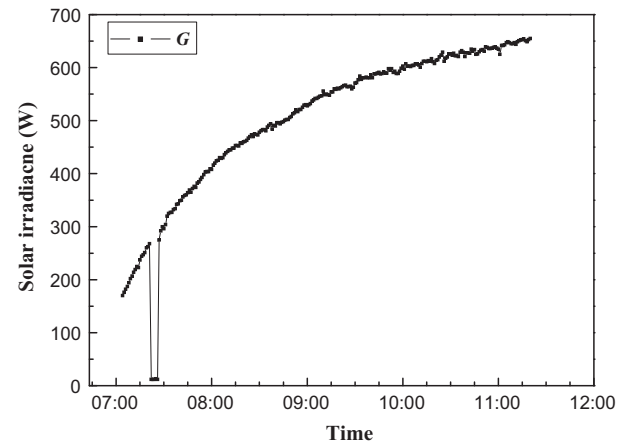


Fig. 4a. Solar irradiance profile in the morning.

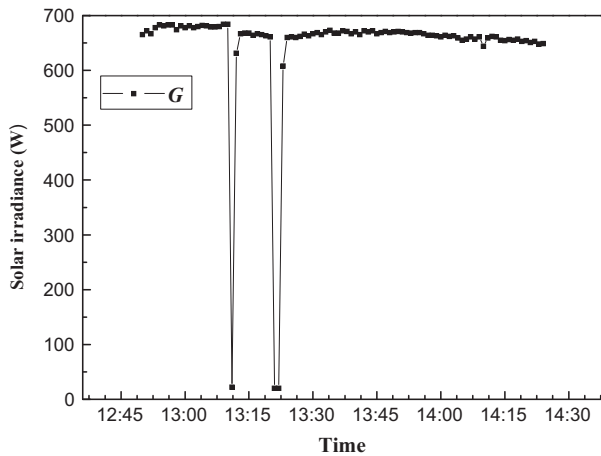


Fig. 4b. Solar irradiance profile in the afternoon.

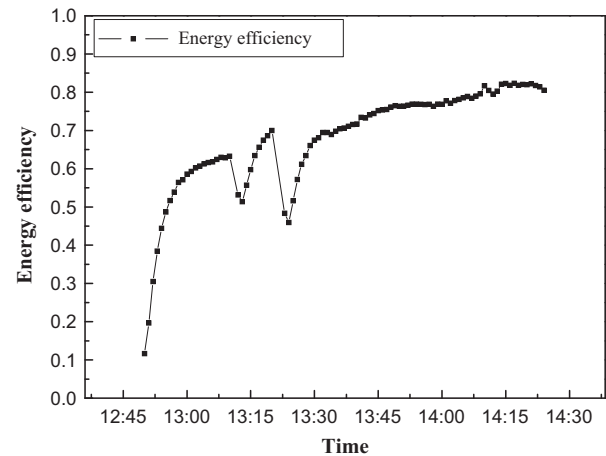


Fig. 5b. Energy efficiency profile during the experimental period.

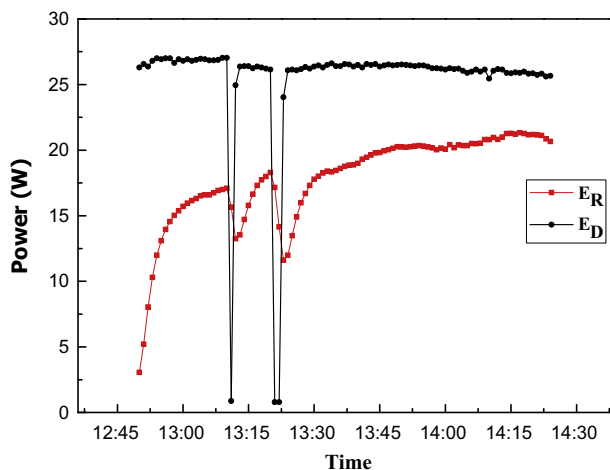


Fig. 5a. Dish power and receiver power profile during the experimental period.

curve presented in Fig. 4a, it is shown that the solar irradiance increases monotonously with time except a fast drop of the solar irradiance is observed at around 7:15 and lasts for 15 min. This could be explained by the fact that a passing cloud. Afterward, there is a quick increase in the solar irradiance. In general, the solar irradiance rises slowly from 160 W/m^2 at 7:00 am to around 650 W/m^2 at 11:30 am. Fig. 4b shows the variation of the solar irradiance from 12:45 pm to 14:35 pm. The results presented in Fig. 4b also clearly show that there exist two low points of the solar irradiance. The reason for this is due to the fact that two short period of passing cloud occurred. From this figure, it can be seen clearly that the solar irradiance is almost unchanged and maintained at around 650 W/m^2 in the afternoon. It is recognized that the constant solar irradiance distribution profile would be reasonable to analyze the energy and exergy performance of the solar receiver. Therefore, a test period of continuous two hours in the afternoon is selected. Dynamic acquisition system is used to record the parameters automatically during the test. The ambient temperature is maintained at around 10°C during the experiment.

Fig. 5a presents a comparison of the power for the concentrated solar radiation and receiver power. For the case of the constant solar irradiance of 650 W/m^2 , the concentrated solar radiation power (E_D) is maintained at around 26.5 kW. In an alternative way, the above observed two low points is lower than 1 kW. In addition, the accurate control system can make sure the reflection

focus located at the aperture of the receiver. The red line shown in Fig. 5a is the receiver power during the testing period. Although the solar irradiance condition is steady, it takes the solar power about 20 min to achieve steady state. It is due to the fact that the receiver tubes are surrounded by the chamotte with high specific heat capability (C_p). At the starting point, the temperature of the receiver is approximately 10°C and the entire receiver needs to be preheated prior to the real test. It is noteworthy that the rising speed of the receiver power is very high within the first 10 min. This phenomenon is very important and should be stress here since the sunshine is limited in the day time, quick start up will make the overall solar power generation system to generate more electricity. Therefore, the cost of the power generation will be lower and the investment recovery period could be shorter. It is very clear that the decrease of the receiver power is very quick, whereas the recovery of the receiver power is very slow. The time for the dish shadowed by the cloud is about 4 min while the recovery time for the receiver is approximately 12 min, which is three times of the shadowed time. These two low points are negative for the receiver, and could form two big attack to the solar generate system. Thus, the site selection of the solar power station should be in some place with strong sunshine and little cloud. After the two low points, the receiver power (E_R) rises slowly and achieves the maximum value of 21.3 kW at the end of the experimental.

The energy efficiency of the receiver is shown in the Fig. 5b. Because the E_D is almost unchanged during the entire test period, the profile of the receiver energy efficiency shows the same trend as the profile of E_R , as shown in Fig. 5a. It is found that when the solar receiver turns into steady state, the efficiency of the solar receiver can be above 70%. The peak value of the efficiency is 82%, and finally, the efficiency is maintained at about 80%.

Fig. 6 demonstrates the evolution of the heat loss factor (U'_L). At the starting point, U'_L is very high (0.55 kW/K) because of the receiver preheating, and then it drops very quickly within the first 10 min. The two peak point is because of the weather, as previously mentioned. When the receiver works at steady state, the heat loss becomes lower and U'_L achieves the minimum value of 0.02 kW/K. The heat loss is mainly due to the thermal convection between the receiver and ambient. The wind speed is very low during the test, as a result, the natural convection is the main way for the heat loss. It can be concluded that the wind is also a crucial factor for the site selection of the solar power station.

Fig. 7a shows the comparison between the receiver exergy (Ex_R) and the concentrated solar energy as well as the receiver energy. From this figure, the exergy rate and energy rate vary in a similar

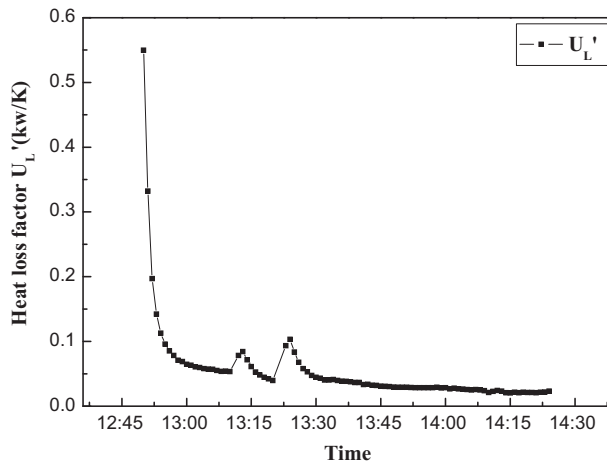


Fig. 6. Heat loss factor profile during the experimental period.

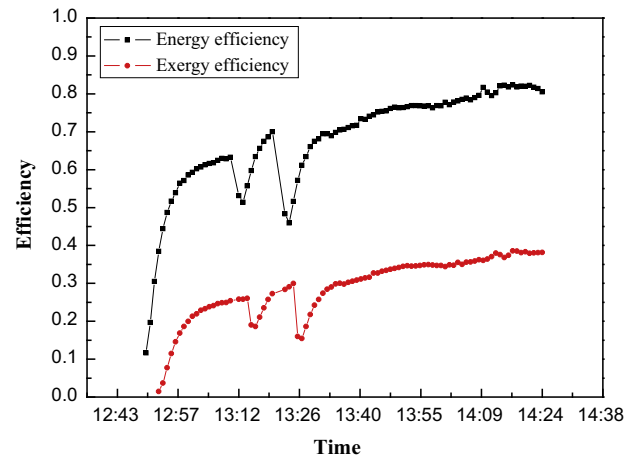


Fig. 7b. Energy and exergy efficiency profile during the test period.

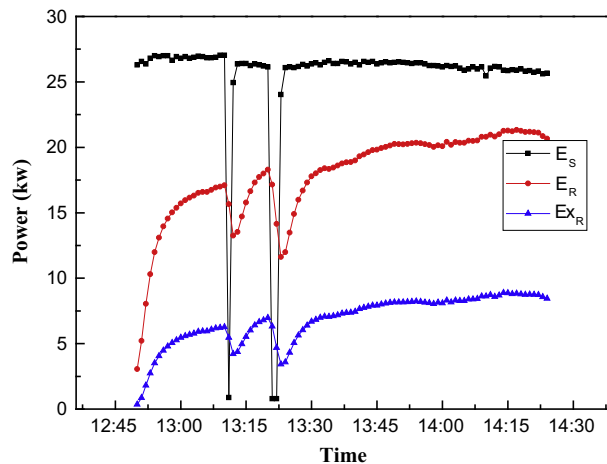


Fig. 7a. Energy and exergy profile of the receiver during the test period.

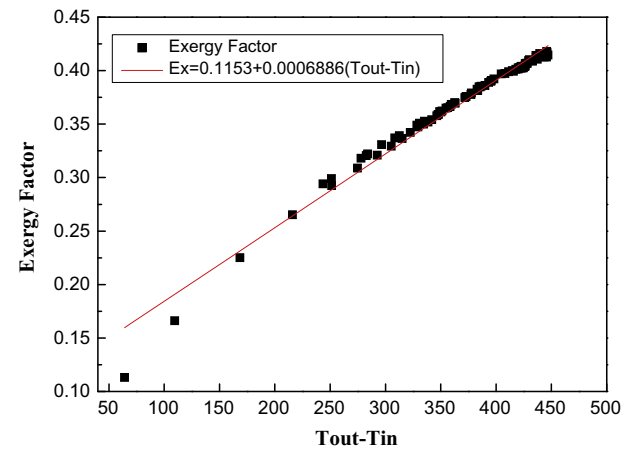


Fig. 8. Exergy factor as function of $T_{out} - T_{in}$.

manner, the passing cloud can also result in the drop of the exergy rate. It is noted that the highest value of the exergy rate during the test period is around 8.8 kW, whereas the maximum energy rate can reach 21.3 kW. It can be concluded that the quality of the energy from the receiver is low due to a large amount of irreversible energy changes such as heat losses and the transfer of high quality radioactive energy to a fluid circulating at a relatively low temperature. From Eq. (13), it can be concluded that under the same temperature difference ($T_{out} - T_{in}$) and the same energy rate $\dot{m}c_{av}(T_{out} - T_{in})$ condition, increasing the receiver inlet temperature (T_{in}) can get higher exergy rate (Ex_R). It will be very helpful for the design of the solar power system. Therefore some recuperator or heat exchanger should be used in the inlet of the solar receiver to recover the waste heat and increase the solar inlet temperature.

Fig. 7b presents the comparison between the energy efficiency and exergy efficiency. It is shown from Fig. 7b that similar trends in the exergy efficiency and the energy efficiency are obtained. The highest exergy efficiency is approximately 38.3%, whereas the highest energy efficiency is around 82%. Comparing with the exergy efficiency (10%) obtained by Ashmore's experiment [27], the current proposed solar receiver achieves better exergy efficiency performance. It is also found that the exergy efficiency is quite lower than the energy efficiency, which implies that lower quality energy obtained from the receiver. This can be explained from Eq. (13), where Ex_R is the exergy rate of the receiver, and

$\dot{m}c_{av}T_{amb} \ln \left(\frac{T_{out}}{T_{in}} \right)$ is the exergy loss to the surroundings. Therefore the magnitude of the exergy rate is strongly depended on the exergy loss expressed as $\dot{m}c_{av}T_{amb} \ln \left(\frac{T_{out}}{T_{in}} \right)$. In the current experiment, the inlet temperature of the receiver is lower than 303 K, whereas the outlet temperature is very high and with the maximum value of 700 K. The temperature ratio (T_{out}/T_{in}) is very high so that too much exergy loss is caused. In this case, the exergy rate Ex_R is very low in the solar system. Accordingly, increasing the inlet temperature could be a potential way to increase the exergy efficiency.

Fig. 8 shows the exergy factor plotted as a function of the temperature difference between the outlet and inlet temperature of the receiver with a linear fitting equation. The exergy factor can also be used as a measure of the performance of the receiver. Obviously, as the temperature difference increases, the exergy factor also increases. This plot suggests that the higher exergy factor can be obtained when high temperature difference is available. As seen from this figure, a lower value of exergy factor (0.3) is obtained even though the temperature difference is high (250 K). The highest exergy factor is 0.41 during the entire test.

5. Conclusions

The thermal performance of a coiled tube solar receiver under real solar radiation condition has been experimentally evaluated

in this work. A parabolic dish with solar tracker system is used in the experiment. The experimental data are analyzed using energy and exergy analyse method. Experimental results revealed that the solar irradiance rises slowly from 160 W/m² to around 650 W/m² in the morning, and keep almost constant at around 650 W/m² in the afternoon. The efficiency of the solar receiver can be above 70%. The peak point of the efficiency is 82%, and generally the efficiency is maintained at about 80%. During the steady state, the heat loss becomes lower and U_f achieves the minimum value of 0.02 kW/K. The highest exergy efficiency is approximately 38.3%, whereas the highest energy efficiency is around 82%. As the temperature difference increases, the impact of the exergy factor increases. A lower value of exergy factor (0.3) is obtained even though the temperature difference is high (250 K). The highest exergy factor is 0.41 during the entire test.

Acknowledgements

The authors would like to acknowledge the financial support from National Natural Science Foundation of China (NSFC No. 51206164).

References

- [1] Steinfeld A. Solar thermochemical production of hydrogen – a review. *Sol Energy* 2005;78:603–15.
- [2] Le Roux WG, Bello-Ochende T, Meyer JP. Operating conditions of an open and direct solar thermal Brayton cycle with optimised cavity receiver and recuperator. *Energy* 2011;36:6027–36.
- [3] Wang M, Siddiqui K. The impact of geometrical parameters on the thermal performance of a solar receiver of dish-type concentrated solar energy system. *Renew Energy* 2010;35:2501–13.
- [4] Grange B, Ferrière A, Bellard D, Vrinat M, Couturier R, Pra F, Fan Y. Temperature air solar absorber based on compact heat exchange technology. *ASME, GT* 2011, vol. 133/031004-1.
- [5] Bader R. Experimental and numerical heat transfer analysis of an air-based cavity-receiver for solar trough concentrators. *ASME J Sol Energy Eng* May 2012;134:021002-1.
- [6] Bader R, Barbato M, Pedretti A, Steinfeld A. An air-based cavity receiver for solar trough concentrators. *ASME J Sol Energy Eng* 2010;132:031017.
- [7] Bader R, Pedretti A, Steinfeld AA. A 9m-aperture solar parabolic trough concentrator based on a multilayer polymer mirror membrane mounted on a concrete structure. *ASME J Sol Energy Eng* 2011;133:031016.
- [8] Lovegrove K, Burgess G, Pye J. A new 500 m² paraboloidal dish solar concentrator. *Sol Energy* 2011;85:620–6.
- [9] Li L, Dubowsky S. A new design approach for solar concentrating parabolic dish based on optimized flexible petals. *Mech Mach Theory* 2011;46:1536–48.
- [10] Wu S, Xiao L, Cao Y, Li Y. A parabolic dish/AMTEC solar thermal power system and its performance evaluation. *Appl Energy* 2010;87:452–62.
- [11] Li Z, Tang D, Du J, Li T. Study on the radiation flux and temperature distributions of the concentrator–receiver system in a solar dish/stirling power facility. *Appl Therm Eng* 2011;31:1780–9.
- [12] Joo H, Dae S, Kim Y, Tae B. Performance comparisons of dish type solar concentrator with mirror arrangements and receiver shapes. In: *Proceedings of ISES solar world congress, solar energy and human settlement*; 2007. p. 706–10.
- [13] Chen L, Zhang W, Sun F. Power efficiency entropy-generation rate and ecological optimization for a class of generalized irreversible universal heatengine cycles. *Appl Energy* 2007;84:512–25.
- [14] Lim S, Kang Y, Lee H, Shin S. Design optimization of a tubular solar receiver with a porous medium. *Appl Therm Eng* 2014;62:566–72.
- [15] Wang M, Siddiqui K. The impact of geometrical parameters on the thermal performance of a solar receiver of dish-type concentrated solar energy system. *Renew Energy* 2010;35:2501–13.
- [16] Antonio L, Jesus F, Felix M. Evaluation of the potential of central receiver solar power plants: configuration, optimization and trends. *Appl Energy* 2013;112:274–88.
- [17] Buck R, Brauning T, Denk T, Pfander M, Schwarzbozl P, Tellez F. Solar-hybrid gas turbine-based power tower systems. *J Sol Energy Eng* 2001;124(1):2–9.
- [18] Kumar NS, Reddy KS. Comparison of receivers for solar dish collector system. *Energy Convers Manage* 2008;49:812–9.
- [19] Hirschier I, Hess D, Lipinski W, Modest M, Steinfeld A. Heat transfer analysis of a novel pressurized air receiver for concentrated solar power via combined cycles. *J Therm Sci Eng Appl* 2009;1:1–6.
- [20] Hirschier I, Hess D, Lipinski W, Modest M, Steinfeld A. Heat transfer analysis of a novel pressurized air receiver for concentrated solar power via combined cycles. *ASME* 2009;1:041002-1.
- [21] Hachicha AA, Rodriguez I, Castro J, Oliva A. Numerical simulation of wind flow around a parabolic trough solar collector. *Appl Energy* 2013;107:426–37.
- [22] Hachicha AA, Rodriguez I, Capdevila R, Oliva A. Heat transfer analysis and numerical simulation of a parabolic trough solar collector. *Appl Energy* 2013;111:581–92.
- [23] Wang P, Liu D, Xu C. Numerical study of heat transfer enhancement in the receiver tube of direct steam generation with parabolic trough by inserting metal foams. *Appl Energy* 2013;102:449–60.
- [24] Yu Z, Feng Y, Zhou W, Jin Y, Li M, Li Z, et al. Study on flow and heat transfer characteristics of composite porous material and its performance analysis by FSP and EDEP. *Appl Energy* 2013;112:1367–75.
- [25] Roldan MI, Valenzuela L, Zarza E. Thermal analysis of solar receiver pipes with superheated steam. *Appl Energy* 2013;103:73–84.
- [26] Kaushik SC, Gupta MK. Energy and exergy efficiency comparison of community-size and domestic-size paraboloidal solar cooker performance. *Energy Sustain Dev* 2008;12:60–4.
- [27] Ashmore M, Simeon HT. Experimental energy and exergy performance of a solar receiver for a domestic parabolic dish concentrator for teaching purposes. *Energy Sustain Dev* 2014;19:162–9.
- [28] Wang D, Lin F. The Impact of the wall thickness on the outer wall temperature in a tubular solar air receiver. In: *Asian conference on gas turbine*; 2012. ACGT2012-5068.
- [29] Mawire A, Taole SH. Experimental energy and exergy performance of a solar receiver for a domestic parabolic dish concentrator for teaching purposes. *Energy Sustain Dev* 2014;19:162–9.
- [30] Macphee D, Dincer I. Thermal modeling of a packed bed thermal energy storage system during charging. *Appl Therm Eng* 2009;29:695–705.
- [31] Petela R. Exergy of undiluted thermal radiation. *Sol Energy* 2003;74:469–88.
- [32] Moffat RJ. Describing the uncertainties in the experimental results. *Exp Therm Fluid Sci* 1988;1:3–17.